

## **Section 5**

Development of and studies with regional and convective-scale atmospheric models and ensembles.



## A Standalone Limited Area Capability for the Finite-Volume Cubed-Sphere Dynamic Core

Thomas L. Black<sup>1</sup>, James A. Abeles<sup>1,2</sup>, Benjamin T. Blake<sup>1,2</sup>, Dusan Jovic<sup>1,2</sup>, Eric Rogers<sup>1</sup>, Ying Lin<sup>1</sup>, Logan C. Dawson<sup>1,2</sup>, Jacob R. Carley<sup>1</sup>

<sup>1</sup>NCEP/EMC College Park, MD, U.S.

<sup>2</sup>IMSG, College Park, MD, U.S.

Email: Tom.Black@noaa.gov

The Next Generation Global Prediction System (NGGPS) of the National Weather Service (NWS) is based on the Finite Volume Cubed-Sphere (FV3) dynamical core (Lin 2004; Putnam and Lin 2007). Models using this core have executed on domains that cover the entire globe. The responsibilities of the NWS include providing forecast guidance on the global scale as well as for more localized regions such as those within the United States and associated territories. Given that FV3 was originally built to run over the globe, a method was needed to focus the prediction over any desired limited area region. FV3 developers addressed this issue by adding a capability to insert a single nest domain within the global parent (Harris and Lin 2013). This configuration requires that the nest run concurrently with its parent to receive boundary updates at each parent timestep. However, if the specific goal is to forecast only for a limited region, then there is significant additional computational expense in also running a parent domain over the entire globe to provide boundary conditions for a nest with limited forecast length (i.e.  $\leq 60$  h). It is also impractical at present for convective-scale ( $\leq 3$  km grid-spacing) data assimilation systems that feature analysis updates at a frequency of  $\leq 1$  hour, as they typically feature earlier data cut-offs than their global counterparts (Gustafsson et al. 2018). In order to avoid cost and data assimilation issues in global forecasts associated with a nest, a limited area or stand-alone regional (SAR) version of FV3 has been constructed. This version has no global parent and thus uses a completely isolated domain with boundary conditions pre-generated from an independent external forecast.

Within the theme of unifying global and regional NWP applications, the same version of the FV3 dynamic core that was enhanced for the standalone limited area capability is also planned for operational implementation in the Global Forecast System (GFS) at the National Centers for Environmental Prediction in 2019 (GFSv15). The uppermost section of source code lying over the forecast model is called the NOAA Environmental Modeling System (NEMS) layer. NEMS uses the Earth System Modeling Framework (Hill et al. 2004, Collins et al. 2005) and includes features providing the means to couple to other modeling systems provided by the National Unified Operational Prediction Capability (NUOPC) layer, which is a set of ESMF-based component templates and interoperability conventions. The forecast integration in the regional mode runs in precisely the same way as in the original global version and thus nearly all the modifications for a limited area forecast are directly or indirectly related to the handling of the domain's boundaries.

Currently EMC is running a regional FV3-SAR forecast with 3 km grid spacing over the CONUS along with a nested domain forecast with identical resolution and areal coverage (Fig. 1). Both forecasts run at 0000 UTC each day out to 60 hours using initial conditions from the 0000 UTC GFSv15 system. The FV3-SAR also leverages the 0000 UTC GFSv15 cycle for lateral boundary conditions, which are specified at a 3 hour interval. Both configurations currently utilize the GFSv15 physics suite for testing purposes.

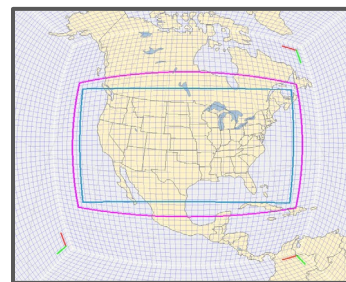


Figure 1. FV3-SAR and FV3-Nest computational domain (pink) and output grid (blue).

Initial comparisons of forecast precipitation verification also demonstrate little practical difference in skill out to 60 forecast hours between the SAR and nested configurations (Fig. 2). This suggests that the lateral boundary conditions are being applied correctly and, at this early stage of development, less frequent boundary updates in the SAR domain appear to not have a detrimental impact on the resulting forecast. Finally, a compelling benefit of the SAR is that it requires significantly less computational resources to run the forecast. The global with a nest simulation runs 1.7x slower using the same number of nodes as the SAR (Fig. 3).

Work on applying data assimilation in this regional system has begun with the long-term goal of developing a convection-allowing, ensemble-based data assimilation and prediction system with at least an hourly-update cadence.

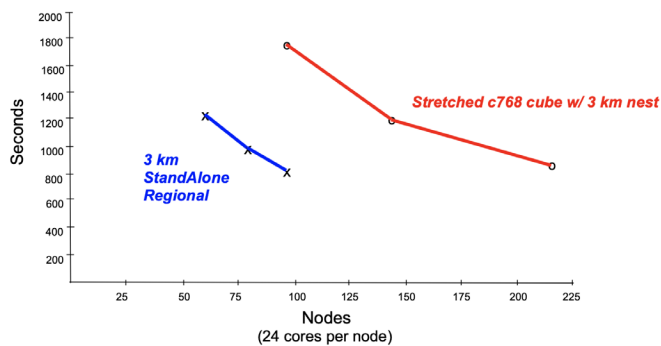


Figure 3. 3 km FV3-SAR (blue) vs. global FV3 with 3 km nest computational time as a function of node count (24 cores per node). No output/history files were written during model integration to minimize the influence of I/O contention.

## References

- Collins, N., and Coauthors, 2005: Design and implementation of components in the Earth System Modeling Framework. *Int. J. High Perform. Comput. Appl.*, **19**, 341–350.
- Gustafsson N., and Coauthors, 2018: Survey of data assimilation methods for convective scale numerical weather prediction at operational centres. *Quart. J. Roy. Meteor. Soc.*, **144**, 1218-1256.
- Harris, L.M. and S. Lin, 2013: A Two-Way Nested Global-Regional Dynamical Core on the Cubed-Sphere Grid. *Mon. Wea. Rev.*, **141**, 283–306.
- Hill, C., C. DeLuca, V. Balaji, M. Suarez, and A. da Silva, 2004: The architecture of the Earth System Modeling Framework. *IEEE Comput. Sci. Eng.*, **6**, 18–28.
- Lin, S., 2004: A “Vertically Lagrangian” Finite-Volume Dynamical Core for Global Models. *Mon. Wea. Rev.*, **132**, 2293–2307.
- Putman, W. M., and S.-J. Lin, 2007: Finite-volume transport on various cubed-sphere grids. *J. Comput. Phys.*, **227**, 55–78.

## FV3NEST vs. FV3SAR 24-h Precipitation Scorecard for FV3NEST and FV3SAR

2018-12-18 00:00:00 – 2019-03-20 00:00:00

		CONUS		
		F36	F60	
ETS	24-h Precip.	> .01 in.	▲	▲
		> .10 in.	▲	▲
		> .25 in.		
		> .50 in.		
		> .75 in.		
		> 1.0 in.		
		> 1.5 in.	■	
		> 2.0 in.		
		> 3.0 in.		
Bias	24-h Precip.	> .01 in.	▲	▲
		> .10 in.	▲	▲
		> .25 in.	▲	
		> .50 in.		
		> .75 in.		
		> 1.0 in.		
		> 1.5 in.		
		> 2.0 in.		
		> 3.0 in.		
> 4.0 in.				

Figure 2. 3 km FV3-NEST vs. 3 km FV3-SAR precipitation scorecard for 24 hour accumulation periods ending at 36 and 60 forecast hours over the CONUS. Statistics cover the period from Dec. 18th, 2018 to March 20th, 2019. Large green (red) triangles indicate FV3-NEST is better (worse) at the 99.9% significance level, small green (red) triangles indicate FV3-NEST is better (worse) at the 99% significance level, green (red) shading indicates FV3-NEST is better (worse) at the 95% significance level.

# Implementation and Evaluation of MG3 microphysics in FV3GFS

Anning Cheng<sup>1,2</sup>, Shrinivas Moorthi<sup>2</sup>, Yu-tai Hou<sup>2</sup>, Jack Kain<sup>2</sup>, Fanglin Yang<sup>2</sup>

1. IMSG, Inc. and 2. EMC/NCEP, NOAA

Email: [Anning.Cheng@noaa.gov](mailto:Anning.Cheng@noaa.gov)

Cloud microphysics is among the key physical processes that drive increases in forecast accuracy for global and regional numerical models. The Morrison and Gettleman double moment microphysics version3 (MG3) is physically comprehensive and computationally efficient within the FV3GFS (Finite-Volume version 3 Global Forecast System) and unified forecast system. MG3 [1] was ported from National Center for Atmospheric Research in February 2018. MG3 forecasts the number concentration and mass mixing ratio of cloud liquid, cloud ice, rain, snow and graupel/hail, and is now the most comprehensive microphysics at EMC. Other two-moment schemes, such as Thompson, do not forecast the number concentration of cloud water, snow, and graupel/hail. That is because in those schemes the numbers do not have local storage, but their mixing ratios do. This internal inconsistency can cause more rain, snow, and graupel/hail to be suspended in the atmosphere column because of the lack of ice nuclei (IN) and cloud condensation nuclei (CCN).

MG3 has many good features: 1) a unified treatment of cloud fraction in radiation and macrophysics, 2) subgrid-scale microphysics, 3) max-overlap and in-cloud precipitation fraction area, and 4) options for subcolumn microphysics. The subgrid-scale microphysics makes MG3 scale-aware. The subcolumn microphysics can be unified with the 3D/subcolumn radiation.

The coupling of MG3 with the aerosol has options for differing complexity, ranging from a simple constant aerosol mixing ratio to being fully coupled with MAM7 (the Modal Aerosol Model). The options are: 1) a constant aerosol mixing ratio, 2) climatology IN/CCN from the Community Atmosphere Model, version 5, 3) climatological aerosol from the Modern-Era Retrospective analysis for Research and Applications, Version2, 4) the Georgia Institute of Technology–Goddard Global Ozone Chemistry Aerosol Radiation and Transport, and 5) MAM7.

MG3 has been coupled with the CS-AW (Chikira Sugiyama-Arakawa Wu) scale-aware deep convection and tested for months to improve their performance. The time series of global mean precipitation, evaporation, and cloud fraction are the basic metrics to test the stability, mass and water vapor conservation, and even scale-awareness for a numerical model. Figure 1 shows the results from a ten-day forecast run starting from 2016/12/06 using C768L65 with CSAW+MG3. The globally mean total precipitation is well balanced with the evaporation. Both are near 3 mm/day and have nice diurnal cycles (1a). The horizontal grid-size for C768 is nearly 13 kms and we expect a scale-aware deep convective scheme should give about the same precipitation as the large-scale precipitation from the microphysics. The large-scale precipitation would exceed the deep convective precipitation with a further increase of the horizontal resolution. Because the initial condition is from data assimilation based on SAS+GFDL microphysics, an initial spin-up with a sudden increase of total precipitation causes the decrease of the global mean precipitable water (1b), which is brought back within a few days. This shows good model stability and good self-adjustment to a premium state. The globally mean low-, middle-, and high-level cloud amount is near 35%, 20%, and 35% (1c), respectively. The total globally mean cloud amount is above 60%. All are in good shape and ready for tune-up for anomaly correlation (AC) score and root mean square score, etc. Limited case studies show that CSAW+MG3 can exceed the operational model in AC score, but more studies are needed.

CSAW+MG3 has also shown a strong ability in hurricane forecasting. A track forecast for hurricane Harvey was performed using FV3GFS initial conditions and ECMWF initial conditions (Figure 2). Harvey landed and hesitated in southern Texas and moved north-east in the best track. However, most numerical prediction models produced a west-moving track. The initial condition from FV3GFS has a strong east-moving signal/forcing and CSAW+MG3 can produce an east-moving Harvey starting from

2017/08/22, which is about 7 days in advance of its sudden eastward move and final landfall in Louisiana. The initial condition from ECMWF has a weak east-moving signal/forcing, but CSAW+MG3 can still produce a northeast moving hurricane starting at 2017/08/26.

Given the relatively recent implementation and testing of MG3, we expect more performance improvement by fixing its systematic biases and bugs in the future. The AC, RMS, and precipitation score will be compared with those from the operational model for a months- to years-long forecasting test.

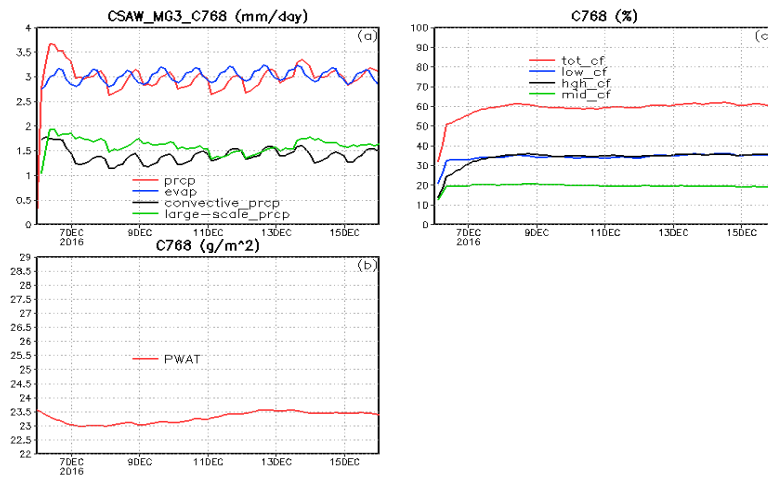


Figure 1. Time series from ten day forecast using CSAW+MG3 with C768L65 resolution.

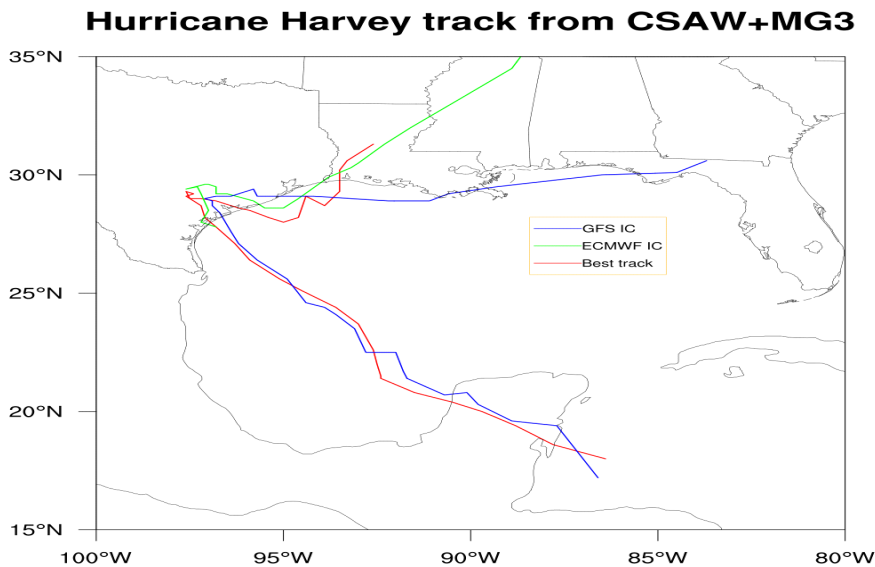


Figure 2. Hurricane tracks from FV3GFS using CSAW+MG3 with C768L65 resolution.

## References

[1] A. Gettelman, H. Morrison, S. Santos, P. Bogenschutz, and P. H. Caldwell: Advanced two-moment microphysics for global models. Part II: Global model solutions and aerosol-cloud interactions. *J. Climate*, **28**, 1288-1307.

# An experiment in numerical prediction of volcanic gas transportation

Akihiro Hashimoto, Takehiko Mori, Toshiki Shimbori and Akimichi Takagi

<sup>1</sup>Meteorological Research Institute, Japan Meteorological Agency, Tsukuba, Japan

## 1. Introduction

The amount and composition of volcanic gas observed in the vicinity of a volcano are closely related to underground hydrothermal processes or gas escaping from magma. Therefore, it is important to estimate the release rate and composition of volcanic gas as precisely as possible in order to monitor and predict the volcano's activity. Since the SO<sub>2</sub> included in volcanic gas is sensitive to uprising of magma, SO<sub>2</sub> measurement is one of the most important aspects in the monitoring of volcanoes.

The Japan Meteorological Agency (JMA) has categorized 111 domestic volcanoes as active, and continuously monitors 50 of them. The release rate of SO<sub>2</sub> is monitored and made available to the public for Mt. Asama, Miyakejima Island, and Mt. Aso by the JMA, and for several other volcanoes by domestic organizations including research institutions, universities, local governments, and also the JMA. In general, the SO<sub>2</sub> release rate is estimated based on a traverse measurement of SO<sub>2</sub> column concentration, using an ultraviolet spectrometer system. However, the applicability of this method is limited by whether or not a traverse route is available for the target volcano, and the frequency of measurement is restricted by the cost of operation. To perform the estimation of SO<sub>2</sub> release rate for more volcanoes with lower operational costs, we are developing an alternative approach, combining a fixed-point measurement of SO<sub>2</sub> column concentration and a numerical model with fine grid spacing. For the first step of the development, a numerical prediction system for volcanic gas transportation has been constructed, based on a numerical weather prediction (NWP) model and a passive tracer trajectory model. This report will provide a description of the system and preliminary results.

## 2. Numerical prediction system for volcanic gas transportation

The system for numerical prediction of volcanic gas transportation has two components: a numerical weather simulation and a tracer trajectory simulation. The former is performed using the JMA's Non-Hydrostatic Model (JMA-NHM; Saito et al., 2006).

Hashimoto et al. (2017) reported on an ongoing weather prediction experiment, for the purposes of meteorological research and of collaboration with other research fields. This experiment has a 2250 × 2250 km computational domain, with a 5-km horizontal resolution, around Japan. For simulations of volcanic gas transportation, this domain is extended to the south and west by 250 km (Domain-1 in Fig. 1a), and a new domain with a 1-km horizontal resolution (Domain-2) is embedded within Domain-1 (Fig. 1a). This domain covers 17 active volcanoes, which include 9 continuously monitored volcanoes in Kyushu and on remote islands. Another domain with a 200-m horizontal resolution (Domain-3) is further embedded into Domain-2 so as to cover Suwanosejima Island (Fig. 1b).

Corresponding author: Akihiro Hashimoto, Meteorological Research Institute, 1-1 Nagamine, Tsukuba, 305-0052, Japan. E-mail: ahashimo@mri-jma.go.jp

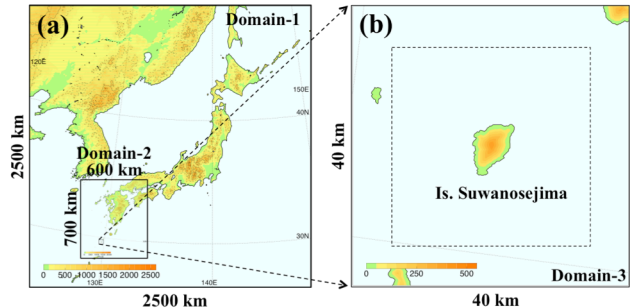


Fig. 1. Computational domains (a) Domain-1, Domain-2 and (b) Domain-3 for weather prediction simulations by 5km-NHM, 1km-NHM and 200m-NHM, respectively. The dotted line shows the domain for the volcanic gas transportation simulation.

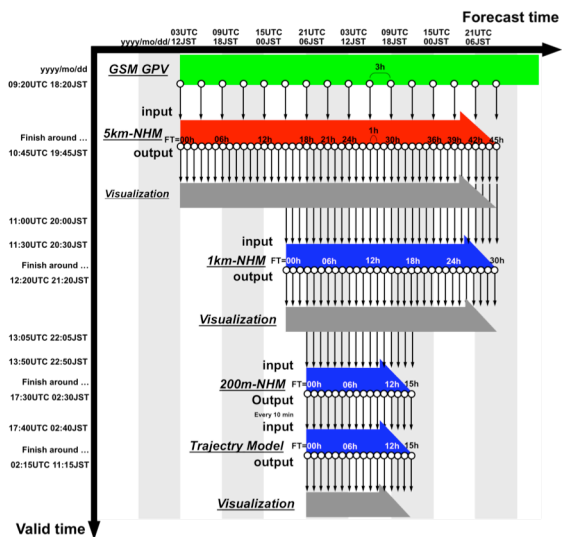


Fig. 2. Schedule for weather prediction, with the initial time of 1200 JST. Thin black arrows indicate the data flow.

The numerical prediction is conducted twice a day. Each time, a simulation is performed in order of Domain-1 (5km-NHM), Domain-2 (1km-NHM), and Domain-3 (200m-NHM). For all the simulations, the Lambert conformal conic projection is adopted, with 30.00 and 60.00°N for the first and second standard latitudes, and 140.00°E for the standard longitude. The vertical grid arrangement and the procedure of time integration in the 5km- and 1km-NHM are the same as those described in Hashimoto et al. (2017).

For the 200-m NHM, the top height of the model domain is 17.7 km. Vertical grid spacing is stretched from 40 m at the

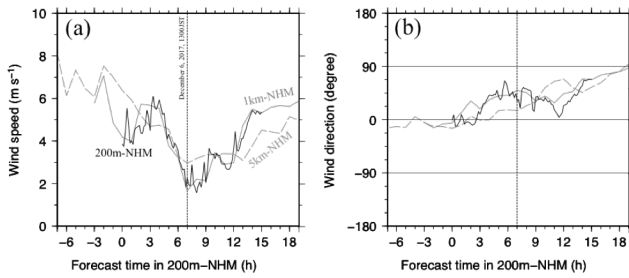


Fig. 3 Time series of (a) surface wind speed and (b) direction at Suwanose Airport, predicted by the 5km- (gray broken line), 1km- (gray solid line), and 200m- (black solid line) NHM. The time interval of the plotted data is one hour for the 5km- and 1km-NHM, and ten minutes for the 200m-NHM. The gray dotted line shows the time of 1300 JST on 6<sup>th</sup> December 2017.

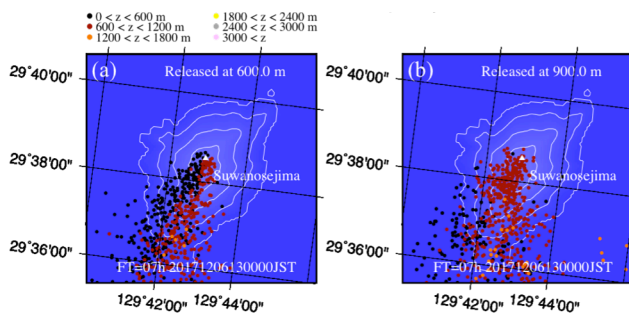


Fig. 4 Distribution of tracers at 1300 JST on 6<sup>th</sup> December 2017, which were released at (a) 600 m and (b) 900 m above the vent. The colors of the dots show the heights of the tracer positions. White contours show the topography.

surface to 199 m at the top of the domain in a terrain-following coordinate system. The total number of vertical layers is 150. The integration time is 15 h, with a timestep of 1 s. The initial and boundary conditions are obtained from the 1km-NHM. The initial time of the 200-m NHM is 3 h later than that of the 1km-NHM (Fig. 2). The boundary condition is provided every hour. Figure 2 shows the schedule and data flow in the numerical prediction, with an initial time of 1200 JST.

The 200-m meshed wind field is output at 10-min intervals within the sub-domain (dotted line in Fig. 1b), in order to perform a simulation of volcanic gas transportation using the passive tracer trajectory model. The simulation period covers the eight days from 3<sup>rd</sup> to 11<sup>th</sup> December 2017, in accordance with the measurements of SO<sub>2</sub> column concentration carried out on Suwanosejima Island during the same period (Mori et al., 2018). In the simulation, the wind field is at first temporally interpolated into a one-second timestep. The wind vector at the position of the tracer is then determined by interpolation of the grid values at the 8 nearest points. The movement of the tracer is predicted by assuming this wind vector is equal to the transfer vector of the tracer. The tracer position is tracked for 15 h unless it goes out of the domain (dotted line in Fig. 1b). In this simulation, 10 tracers are released every 30 s at each of 8 different levels above the vent (from 600 to 1300 m above sea level, at intervals of 100 m).

### 3. Results and discussion

#### 3.1 Sensitivity of predicted surface wind to a horizontal resolution

Figure 3 shows the surface wind speed and direction at Suwanosejima Airport, predicted by simulations with different horizontal resolutions. The 1-km and 200-m NHM show almost same temporal change of the wind. However, wind prediction with the 5km-NHM is clearly different from the others. As the area of Suwanosejima Island is 27.61 km<sup>2</sup>, and its width is about 8 km at most, the 5km-NHM is not able to resolve the topography, which means that the applicability to SO<sub>2</sub> transportation of a wind field of the 5km-NHM is quite limited. Although the results from the 1km- and 200m-NHM show good agreement, it is still unclear if these horizontal resolutions are sufficiently fine to provide accurate wind fields for volcanic gas transportation, because the topography in the model is smoothed so as to stabilize the numerical simulations. To resolve this issue will require more systematic observations of the surface wind, as well as more sensitivity simulations.

#### 3.2 Application to volcanic gas measurement activity

Figure 4 shows a part of the prediction results for SO<sub>2</sub> transportation. The direction and width of the gas plume change depending on the release height. This is due to vertically-sheared environmental wind and topographic effects. In field observations (Mori et al., 2018), it was hard for the crews to determine the main axis of the gas plume, or how broad it was. The numerical prediction system is a useful tool to update crews with concrete predictions of the gas plume, although these predictions have potential errors originating from uncertainties in the release height and other factors. Combining a numerical prediction with well-designed observations, it would be possible to constrain this uncertainty.

### 4. Summary

A numerical prediction system was established, based on the JMA-NHM, for predicting SO<sub>2</sub> transportation. This report has described the procedure of numerical prediction, and presented preliminary results. The predicted surface wind changes depending on the horizontal resolution. By combining a fixed-point measurement of SO<sub>2</sub> column concentration with the numerical prediction of SO<sub>2</sub> transportation, a new approach to evaluating the SO<sub>2</sub> discharge rate can be developed.

### References

- Saito, K., T. Fujita, Y. Yamada, J. Ishida, Y. Kumagai, K. Aranami, S. Ohmori, R. Nagasawa, S. Kumagai, C. Muroi, T. Kato, H. Eito, and Y. Yamazaki, 2006: The operational JMA nonhydrostatic mesoscale model. *Mon. Wea. Rev.*, **134**, 1266–1298.
- Hashimoto, A., M. Niwano, T. Aoki, H. Motoyoshi, S. Yamaguchi, and S. Nakai, 2017: Numerical weather prediction experiment in collaboration with research activities in glaciology and snow disaster prevention. *CAS/JSC WGNE Research Activities in Atmospheric and Oceanic Modelling*, **47**, 5-11.
- Mori, T., E. Shinohara, A. Sugai, D. Mitsunaga, A. Hashimoto, and K. Yamamoto, 2018: Demonstration experiment towards automatic measurement for the SO<sub>2</sub> emission rate. *Disaster Prevention Research Institute Annuals*, **61B**, 344-350.

# Numerical simulation of shallow cloud formation in the United Arab Emirates

Akihiro Hashimoto<sup>1</sup>, Narihiro Orikasa<sup>1</sup>, Takuya Tajiri<sup>1</sup>, Yuji Zaizen<sup>1</sup>, and Masataka Murakami<sup>2,1</sup>

<sup>1</sup>Meteorological Research Institute, Japan Meteorological Agency, Tsukuba, Japan

<sup>2</sup>Institute for Space-Earth Environmental Research, Nagoya University, Nagoya, Japan

## 1. Introduction

We conducted ground-based observations to evaluate the frequency of occurrence of seedable clouds (Hashimoto *et al.*, 2017a), and airborne seeding experiments to investigate the effects of seeding in clouds (Orikasa *et al.*, 2019). This work was undertaken as part of the research project “Advanced Study on Precipitation Enhancement in Arid and Semi-Arid Regions”, funded by the United Arab Emirates (UAE) Research Program (UAEREP) for Rain Enhancement Science. Numerical simulations were performed using a numerical weather prediction model; the objective was to predict the observed clouds for the purposes of model performance evaluation. This report presents preliminary results of the numerical simulations.

## 2. Numerical simulation

Numerical simulations were performed using the Japan Meteorological Agency Non-Hydrostatic Model (JMA-NHM, Saito *et al.*, 2006) with modifications, mainly related to land-surface configuration, as described by Hashimoto *et al.* (2017b). Initial simulations used a 5-km horizontal resolution (5km-NHM); these were followed by simulations with a 1-km horizontal resolution (1km-NHM), as described by Hashimoto *et al.* (2017a). Additional simulations were performed with a 200-m horizontal resolution (200m-NHM) to reproduce fine-scale cloud convection in the area targeted for seeding experiments.

Corresponding author: Akihiro Hashimoto, Meteorological Research Institute, 1-1 Nagamine, Tsukuba, 305-0052, Japan. E-mail: ahashimo@mri-jma.go.jp

## 3. Results

The calculated air temperature time series (1km-NHM) were compared to an observed air temperature time series collected at Al Ain international airport (Fig. 2a,b). Diurnal air temperature variations were observed that extended from the surface of the

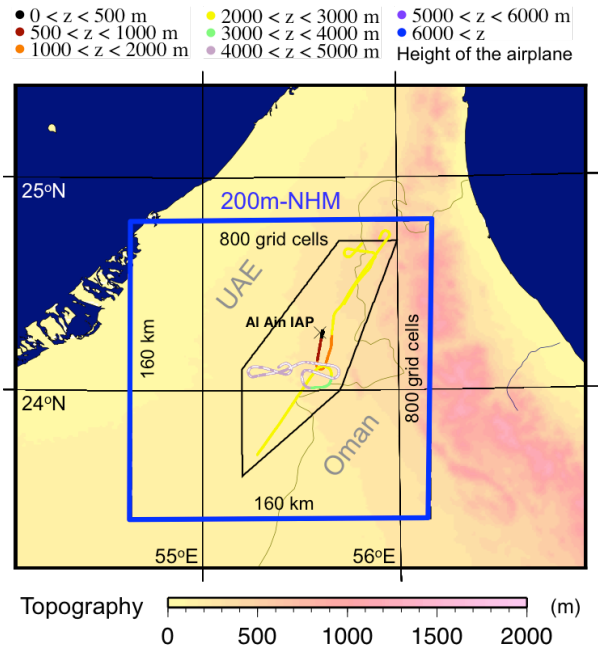


Fig. 1. Computational domain for the 200m-NHM (blue line). Colored dots show the flight path and the height of airplanes.

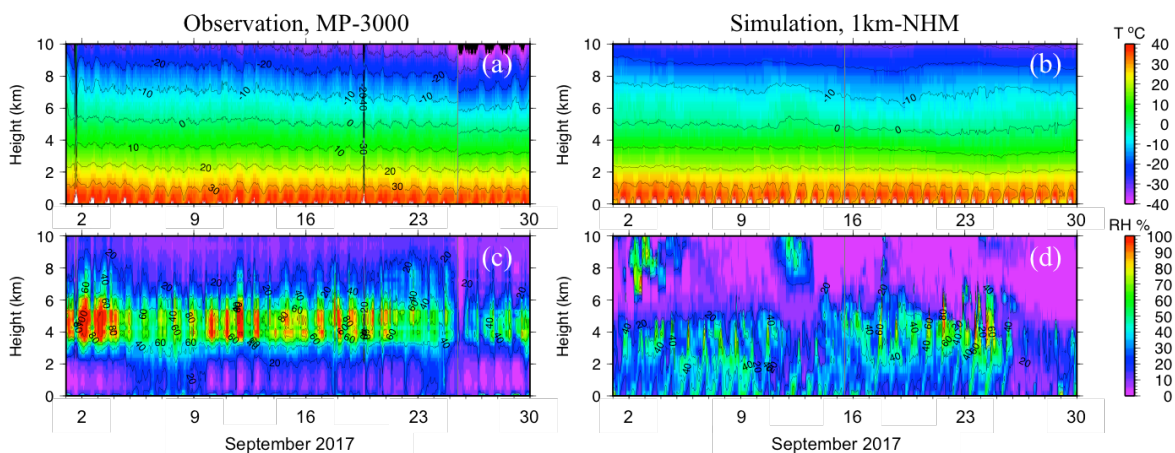


Fig. 2. Time series vertical profiles for September 2017. (a) observed air temperature; (b) simulated air temperature; (c) observed relative humidity; (d) simulated relative humidity. Observations were performed using a multi-wavelength microwave radiometer (MP-3000, Radiometrics) at Al Ain international airport. Simulation results are from the 1km-NHM.

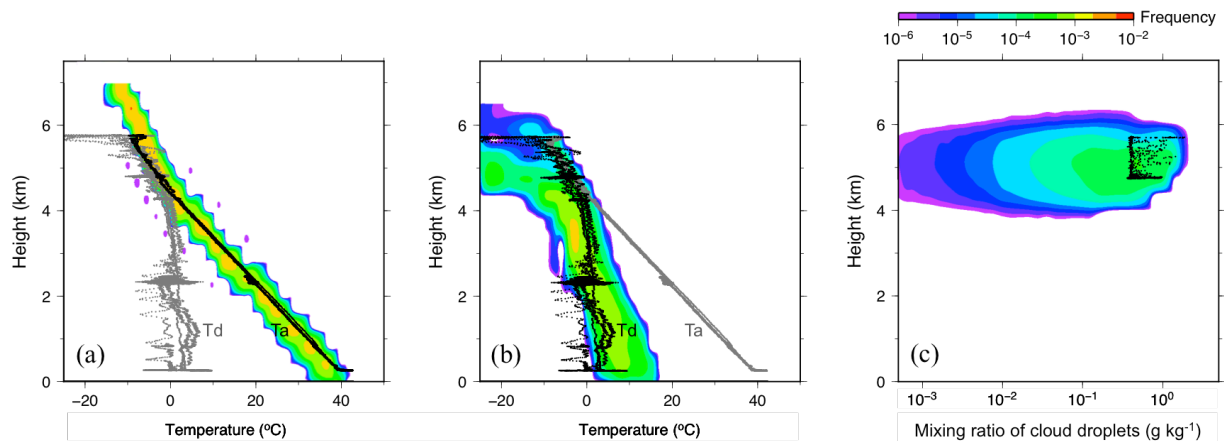


Fig. 3 Frequency of occurrence of simulated: (a) air temperature (Ta); (b) dew point temperature (Td); and (c) mixing ratio of cloud droplets on 21 September 2017. Color indicates the frequency of occurrence. The results were evaluated within the area enclosed by the solid black line in Fig. 1. Black or grey dots show the observed data. Simulation results are from the 200m-NHM.

Earth to 5 or 6 km height. The calculated and observed amplitudes of diurnal air temperature variations matched well at heights of less than 2 km above the Earth's surface, but the calculated amplitude was smaller than the observed amplitude for the middle troposphere. The relative humidity was overestimated in the lower layers of the simulations (Fig. 2c,d). The observed relative humidity was highest at heights between 3 and 6-km height throughout the period of observation. This feature is not clearly seen in the simulations, which is taken to indicate that the thermodynamically-driven circulation in the boundary layer, or turbulent fluxes of heat and moisture at the surface, are not reproduced well by the model. Despite these issues, the maximum predicted relative humidity between the 17th and 22nd September 2017 at around 3-km height agrees well with the observed humidity. A seeding experiment was performed on the 17th, 18th, 20th and 21st September, so it is possible to use predictions on these dates to test the numerical simulations of cloud seeding. We performed control simulations (no-seeding) for these four dates using the 200m-NHM embedded in the 1km-NHM. Preliminary results for the 21st September are presented below.

The observed air temperature, dew point temperature and mixing ratio of cloud droplets were compared to the results of the 200m-NHM simulation (Fig. 3). Black dots show the observed air temperature profile along the airplane flight path shown by colored dots in Fig. 1 (Fig. 3a); the color indicates the frequency of occurrence of simulated air temperature in the area enclosed by the black line in Fig. 1. There is good agreement between the observation and simulation (Fig. 3a). A similar approach was taken for simulation of dew point temperature (Fig. 3b). The simulations successfully predict the observed dry layers below 4.5 km height, and the water vapor saturated layers above 4.5 km height. The highest concentrations of cloud water in the water vapor saturated layer are observed to be of the order of 1 g

kg<sup>-1</sup> (Fig. 3c). The model reproduces this feature successfully. In future work, we will compare the concentration of cloud droplets and other microphysical features in the simulations to the observations (Orikasa *et al.*, 2019), and improve the results by adjusting microphysical parameters in the model.

#### Acknowledgements

This study was conducted as a part of the project "Advanced Study on Precipitation Enhancement in Arid and Semi-Arid Regions" that is supported by the UAERP for Rain Enhancement Science, an initiative of the Ministry of Presidential Affairs, under the management of the National Center of Meteorology and Seismology.

#### References

- Hashimoto, A., N. Orikasa, T. Tajiri and M. Murakami, 2017a: Numerical prediction experiment over the United Arab Emirates by using JMA-NHM. *CAS/JSC WGNE Research Activities in Atmospheric and Oceanic Modelling*, **47**, 5.07-5.08.
- Hashimoto, A., M. Murakami and S. Haginoya, 2017b: First application of JMA-NHM to meteorological simulation over the United Arab Emirates. *SOLA*, **13**, 146-150, doi:10.2151/sola.2017-027.
- Orikasa, N., M. Murakami, T. Tajiri, Yuji Zaizen, and Taro Shinoda, 2019: In situ measurements of aerosol and cloud microphysical properties and cloud seeding experiments over the UAE. *Proceedings of Japan Geoscience Union Meeting 2019*, A-CG41-P01.
- Saito, K., T. Fujita, Y. Yamada, J. Ishida, Y. Kumagai, K. Aranami, S. Ohmori, R. Nagasawa, S. Kumagai, C. Muroi, T. Kato, H. Eito, Y. Yamazaki, 2006: The operational JMA nonhydrostatic mesoscale model. *Mon. Wea. Rev.*, **134**, 1266-1298.

## **NWS HYSPLIT atmospheric transport and dispersion modeling**

Jeff McQueen<sup>1</sup>, Barbara Stunder<sup>2</sup>, Ariel Stein<sup>2</sup>, Ho-Chun Huang<sup>3</sup> and Jack Kain<sup>1</sup>

<sup>1</sup>NWS/NCEP/EMC – College Park, MD

<sup>2</sup>NOAA/OAR/ARL – College Park, MD

<sup>3</sup>IMSG – College Park, MD

Email: Jeff.McQueen@noaa.gov

Understanding and predicting atmospheric transport and dispersion is essential for protecting the health and welfare of the public and emergency response personnel when harmful substances are released into the air in significant quantities. The Federal National Response Framework, approved by the President in January 2008, assigns to NOAA the responsibility for atmospheric transport and dispersion (ATD) prediction of smoke and radioactive and hazardous materials, maintenance and development of HYSPLIT, and coordination with the World Meteorological Organization on international incidents. The NOAA Air Resources Laboratory (ARL) develops many of NOAA's capabilities for these services in conjunction with NCEP.

Currently, the HYSPLIT system is used to provide the following operational atmospheric dispersion products:

- 48-hour wild-fire smoke forecasts from the daily 06 UTC cycle for CONUS, Alaska, and Hawaii, driven by the 12 km North American Model (NAM).
- 48-hour dust forecasts from the 06 and 12 UTC model cycles for CONUS.
- 48-hour volcanic ash forecasts whenever requested by the International Civil Aviation Organization (ICAO)-designated U.S Volcanic Ash Advisory Centers (in Washington, DC and Anchorage, AK). This is typically driven by the NWS Global Forecast System (GFS), although other model output can be used.
- 72-hour radiological emergency response plume forecasts when requested per the World Meteorological Organization (WMO)-designated Regional Specialize Meteorological Center (RSMC) arrangements. This forecast is typically driven by the GFS.
- 16-hour dispersion forecasts for HAZMAT-type (chemical spill, explosion, etc.) incidents upon the request of an NWS Weather Forecast Office (WFO), almost always driven by 12-km NAM, though other model output can be used.
- Back-tracking products when requested per the WMO/RSMC or Comprehensive Test Ban Treaty Organization (CTBTO) agreements. This forecast is typically driven by the GFS, although the NAM can be used.

For all applications, dispersion is simulated using either the multi- or single-processor version of the same code. The smoke and dust forecast guidance is sent in gridded form to the NOAA National Display and Graphics System (NDGD) for distribution to forecasters and emergency managers at the individual state level.

The RSMC predictions are initiated by the NCEP SDM (Senior Duty Meteorologist) and distributed to National Forecast Centers via fax. Digital and graphical products are also shared between other country RSMCs through a protected ARL (non-operational) web page. Monthly exercises are performed by the SDM with other RSMCs.

The volcanic ash predictions are initiated by NCEP, NESDIS/SAB (Synoptic Analysis Branch), or NWS AAWU (Alaska Aviation Weather Unit).

The HAZMAT-type output is made available on a secure NCEP server (<https://hysplit.ncep.noaa.gov/>).

Recently, HYSPLIT volcanic ash products were improved to provide trajectories, and meet NOAA requirements for back-tracking support to the Comprehensive Test Ban Treaty Organization (CTBTO). Improvements soon to be implemented are the use of higher resolution global meteorological FV3GFS gridded predictions and the use of the High Resolution Rapid Refresh (HRRR) model to drive HYSPLIT.

## NOAA's National Air Quality Forecast Capability for Ozone and Fine Particulate Matter

Jeffery McQueen<sup>1</sup>, Pius Lee<sup>2</sup>, Ivanka Stajner<sup>1</sup>, Jack Kain<sup>1</sup>, Jianping Huang<sup>3</sup>, Ho-Chun Huang<sup>3</sup> and Li Pan<sup>3</sup>

<sup>1</sup>NWS/NCEP/EMC – College Park, MD

<sup>2</sup>NOAA/OAR/ARL – College Park, MD

<sup>3</sup>IMSG – College Park, MD

Email: Jeff.McQueen@noaa.gov

The NOAA National Air Quality Forecast Capability, NAQFC, provides two day model forecasts of ozone and fine particulate matter surface concentrations twice per day at the 06 and 12 UTC cycles. The NAQFC operational forecast for ozone (O<sub>3</sub>) for the nation was implemented in September 2007 and for fine particulate matter (PM<sub>2.5</sub>) in January 2015 (Lee, et al., 2017). The NAQFC is made up of the North American Non-Hydrostatic Multiscale Model (NAM-NMMB) 12 km numerical weather prediction model and the EPA Community Model for Air Quality (CMAQ) using Carbon Bond-V (CB-V) gas phase chemistry and AERO-VI particulate matter processing (Fig. 1). Predictions are available in real-time for the continental U.S., Alaska and Hawaii.

Offline coupling between NAM and CMAQ is achieved at hourly intervals by interpolation from the NAM to the CMAQ horizontal and vertical grids. Anthropogenic emissions are updated monthly from the EPA National Emission Inventory for the base year 2014V2. Wild fire smoke emissions were included in 2015 and are based on the U.S. Forest Service BlueSky smoke emission system and the NESDIS Hazardous Mapping System (HMS) fire locations which are updated daily. Dust emissions were also included in 2015 using a friction velocity- and soil moisture criteria-based approach. Dust lateral boundary conditions are provided by the NCEP NEMS Global Aerosol Capability (NGAC) V2 with climatological values from NASA GEOS-Chem for other species (Lu, et al., 2016; Wang, et al., 2018). The number of vertical levels was increased to 35 and an analog bias correction for PM<sub>2.5</sub> was implemented in 2016, with upgrades to CMAQ (to V5.0.2), emissions and PM<sub>2.5</sub> bias correction (Huang, et al., 2017) implemented in 2017 and inclusion of ozone bias correction in 2018. Predictions are available to U.S. state air quality forecasters and the public from the NWS National Digital Guidance Database (NDGD): <http://airquality.weather.gov/> with experimental model predictions at <http://www.emc.ncep.noaa.gov/mmb/aq/>.

In 2018, a Kalman Filter Analog bias correction was improved to capture rare events and extended to both ozone and PM<sub>2.5</sub>. Oil and gas sector emissions were also updated. Tests with a Unified Forecast System (UFS) based on global Finite Volume (FV3) model predictions were begun. In 2019, smoke emissions from the NOAA/NESDIS Global Biomass Burning Emissions Product (GBBEPx) with fire radiative power (for plume rise) will be coupled to NAM-CMAQ as well as NGAC V3. NGACV3 is based on FV3GFS dynamic core inline aerosol global model at ~ 25 km out to 5 days with expected implementation in 2020. These changes to NAM-CMAQ along with updates to anthropogenic emissions and the extension of regional forecasts to 72 hours are also expected to be implemented in 2020.

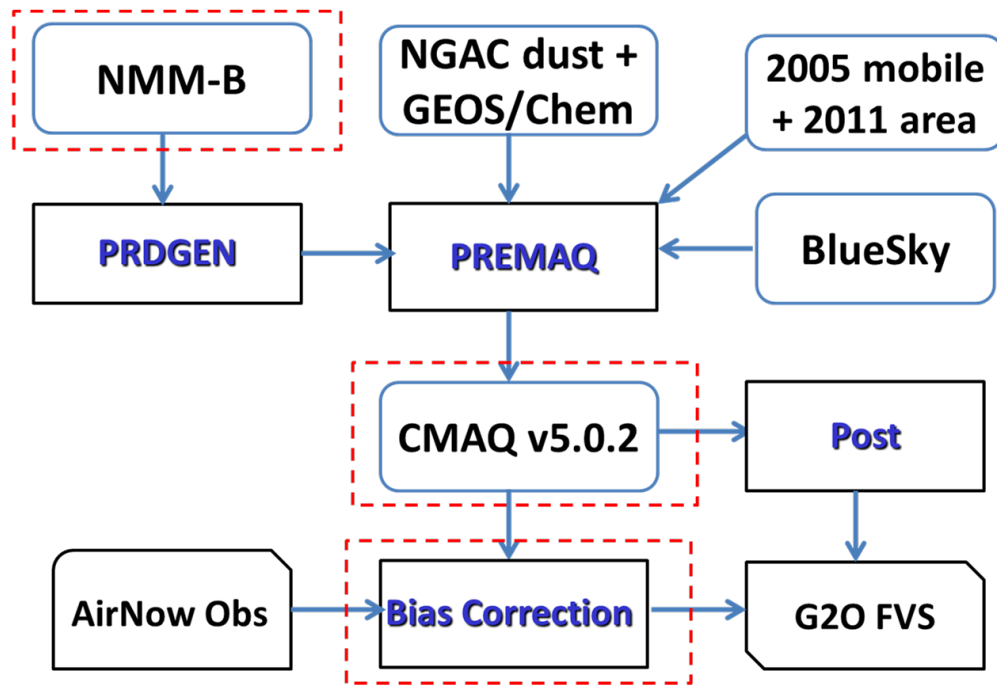


Figure 1. Overview of NAQFC NAM/NMMB-CMAQ system. CMAQ was upgraded to V5.0.2 and bias correction was improved to a Kalman Filter Analog (KFAN) technique in 2017 and 2018.

Huang, J., J. McQueen, J. Wilczak, I. Djalalova, I. Stajner, P. Shafran, D. Allured, P. Lee, L. Pan, D. Tong, H.-C. Huang, G. DiMego, S. Upadhyay, L. Delle Monache. (2017) Improving NOAA NAQFC PM2.5 predictions with a bias correction approach. *Wea. Forec.*, 32,2. DOI: <http://dx.doi.org/10.1175/WAF-D-16-0118.1>

Lee, P., and Coauthors, 2017: NAQFC developmental forecast guidance for fine particulate matter (PM2.5). *Wea. Forecasting*, doi:<https://doi.org/10.1175/WAF-D-15-0163.1>.

Lu, C.-H., A. da Silva, J. Wang, S. Moorthi, M. Chin, P. Colarco, Y. Tang, P. S. Bhattacharjee, S.-P. Chen, H.-Y. Chuang, H.-M. H. Juang, J. McQueen, and M. Iredell, 2016: The implementation of NEMS GFS Aerosol Component (NGAC) Version 1.0 for global dust forecasting at NOAA/NCEP, *Geosci. Model Dev. Discuss.*, 9, 1-37.

Wang, J., Bhattacharjee, P. S., Tallapragada, V., Lu, C.-H., Kondragunta, S., da Silva, A., Zhang, X., Chen, S.-P., Wei, S.-W., Darmenov, A. S., McQueen, J., Lee, P., Koner, P., and Harris, A.: The implementation of NEMS GFS Aerosol Component (NGAC) Version 2.0 for global multispecies forecasting at NOAA/NCEP – Part 1: Model descriptions, *Geosci. Model Dev.*, 11, 2315-2332, <https://doi.org/10.5194/gmd-11-2315-2018>, 2018.

# NCEP HMON-based hurricane ensemble forecast system

Weiguang Wang<sup>1</sup>, Lin Zhu<sup>1</sup>, Hyun-Sook Kim<sup>1</sup>, Dan Iredell<sup>1</sup>, Jili Dong<sup>1</sup>, Zhan Zhang<sup>1</sup>, Avichal Mehra<sup>2</sup>, Vijay Tallapragada<sup>2</sup>  
<sup>1</sup>IMSG at EMC/NCEP/NWS/NOAA, College Park, MD 20740 <sup>2</sup>EMC/NCEP/NWS/NOAA, College Park, MD 20740  
 Email: Weiguang.Wang@noaa.gov

## 1. Introduction

A non-hydrostatic hurricane model has been built at NCEP/EMC, known as the HMON (Hurricanes in a Multi-scale Ocean-coupled Non-hydrostatic) model. HMON replaced the GFDL hurricane model in operational forecasts in July 2017. Meanwhile, a HMON-based ensemble system (HMON-ENS) was also built and real-time experimental runs were made during the hurricane season for two years. The ensemble method is a useful approach for representing model errors and to potentially improve model performance, given that uncertainties in the forecasts and simulations of tropical cyclone track, intensity, and structure are still significant. In addition to improving HMON performance, HMON-ENS experiments can help quantify the uncertainties and sensitivities of the relatively new HMON model when investing resources for further improvement. HMON-ENS provides products for the multi-model ensemble exercise. Next, we will briefly describe the HMON-ENS system and its performance.

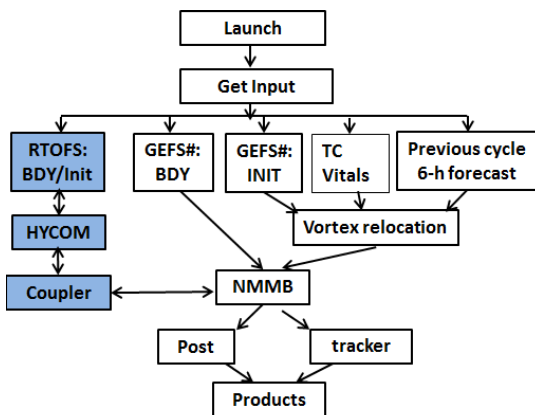


FIG. 1 Flow chart of NCEP HMON-ENS

Table 1 Physics options in members of HMON-ENS

member	Domains	CU	PBL	Land	Cd,Ch	MP
Control (00)	D1:	Scale_SAS	EDMF	NOAH	ICOEf=10	Fer_hires
01	451x451	SAS	EDMF	NOAH	ICOEf=10	Fer_hires
02	D2:	BMJ	EDMF	NOAH	ICOEf=10	Fer_hires
03	231x201	Scale_SAS	GfSPBL	NOAH	ICOEf=10	Fer_hires
04	D3:	Scale_SAS	EDMF	SLAB	ICOEf=10	Fer_hires
05	381x345	Scale_SAS	EDMF	NOAH	ICOEf=10	WSM6
06	NZ=51	Scale_SAS	EDMF	NOAH	ICOEf=6	Fer_hires
07	18 Km	Scale_SASumix	EDMF-A	NOAH	ICOEf=10	Fer_hires
08	6 Km	Scale_SASumix	EDMF-A	NOAH	ICOEf=6	Fer_hires
09	2 Km	SAS	EDMF	NOAH	ICOEf=10	WSM6
10*	# uses FV3GFS data for IC/BC	Scale_SAS	EDMF	NOAH	ICOEf=10	Fer_hires

## 2. HMON-based ensemble system

The operational deterministic HMON system (Mehra et al., 2018) contains two major components (Fig 1). The atmospheric component uses the Non-hydrostatic Multi-scale model on a B grid (NMMB) as its dynamic core. It is configured as triple-nested regional domains, with one parent domain and two movable nests. The model has 51 vertical levels, with horizontal resolution of the three domains being 18, 6, and 2 km, respectively (Table 1). The ocean is simulated by HYCOM, coupled to NMMB through a coupler developed at NCEP. Large scale data are provided by the operational Global Forecast System (GFS) and the Real-Time Ocean Forecast System (RTOFS). The HMON-ENS configuration is the same as the operational HMON except (1) the NCEP operational Global Ensemble Forecast System (GEFS) (a control plus 9 members) and FV3GFS analysis and forecast are used to provide initial and boundary conditions for each member, (2) random perturbations are added to the TC intensity and location, and (3) different PBL, convection, microphysics, and land (sea)-atmosphere interaction schemes are used in the members (Table 1).

## 3. Results and discussions

HMON-ENS was run in real-time during the 2018 hurricane season. Due to limited resources, not all cycles of all storms were simulated. We had 148 verifiable cycles in total for six storms (Debby, Florence, Gordon, Isaac, Kirk, and Michael) in the North Atlantic basin and 76 cycles for two storms (Hector and Lane) in the East Pacific basin. For the Northern Atlantic basin, the statistics of track and intensity errors from the control

member are close to those from the operational HMON. The ensemble mean track and intensity from HMON-ENS are better than the operational HMON (Fig. 2). This was our expectation when HMON-ENS was designed.

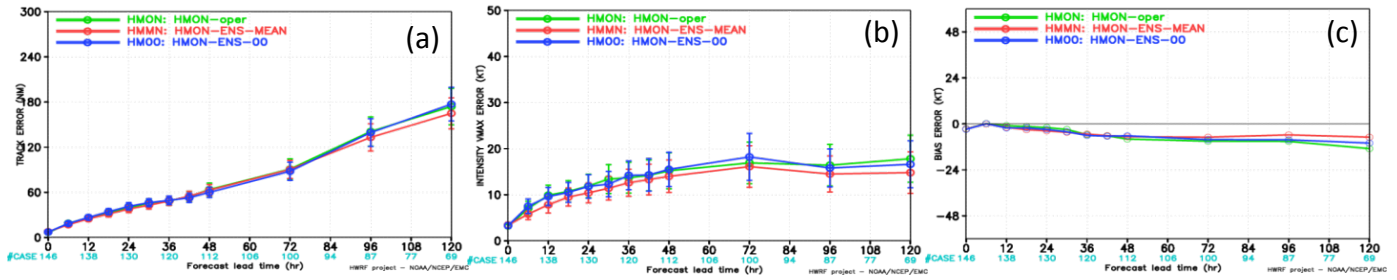


FIG. 2 Comparison of (a) track and (b) intensity errors and (c) bias from operational HMON (green), ensemble mean (red), and control member (blue).

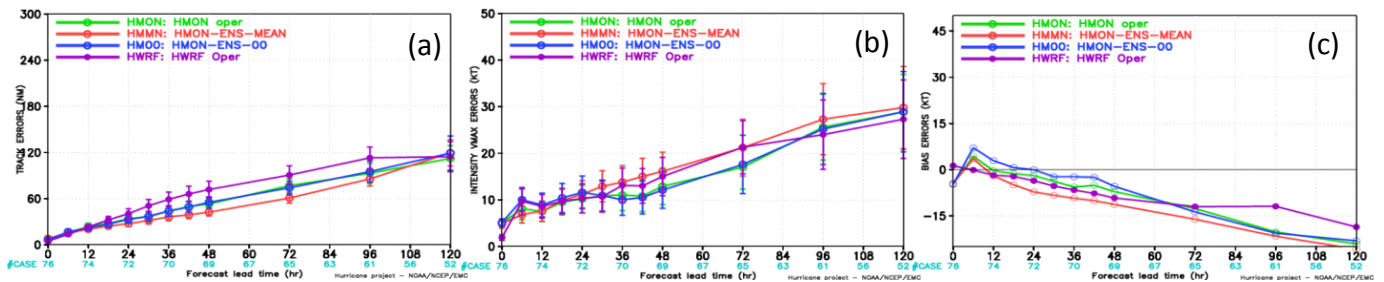


FIG. 3 As in Fig.2 except for East Pacific Basin.

For the Eastern Pacific basin, HMON-ENS generated the best track forecasts. It is even much better than those from the state-of-the-art HWRf. But for intensity forecasts, HMON-ENS did not yield better results than the operational HMON and control member (Fig. 3). This might suggest that we need to take a closer look at the performance of members and make further adjustments.

Compared with the deterministic HMON, HMON-ENS has an advantage in forecasting rapid intensification (RI) of TCs. Analyses suggested that HMON-ENS can capture RI better than the operational HMON (Fig. 4). In Fig 4, HMON-ENS forecast RI for a given cycle is very likely (or likely) when more than 50% (or 30%) of members exhibit RI.

#### 4. Conclusions

In general, as expected, the performance of HMON-ENS is better than the operational HMON. Analyses of individual members suggest that most members performed worse than the well-tuned operational HMON, but results from the averages of all members are the best. The results give us confidence that HMON-ENS improves the multi-model ENS for probabilistic guidance. Further work will focus on adjustments of members to improve intensity forecast.

#### References:

Mehra, A., V. Tallapragada, Z. Zhang, B. Liu, L. Zhu, W. Wang and H. Kim, 2018, Advancing the State of the Art in Operational Tropical Cyclone Forecasting at NCEP, *Tropical Cyclone Research and Review*, Vol 7(1), 51-56

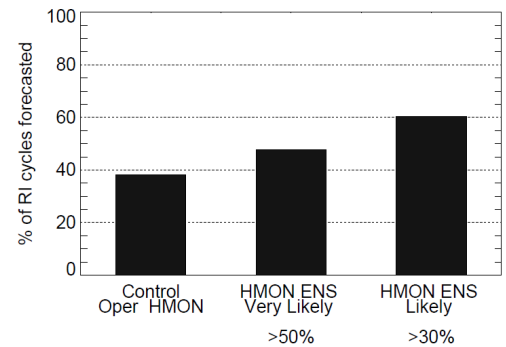


FIG. 4 Percentage of observed RI cycles captured by operational HMON and HMON-ENS.

# NCEP HWRF-based Hurricane Ensemble Prediction System

Zhan Zhang<sup>1</sup>, Weiguo Wang<sup>1</sup>, Lin Zhu<sup>1</sup>, Bin Liu<sup>1</sup>, Keqin Wu<sup>1</sup>, Avichal Mehra<sup>2</sup>, Vijay Tallapragada<sup>2</sup>  
<sup>1</sup>IMSG at EMC/NCEP/NWS/NOAA, College Park, MD 20740 <sup>2</sup>EMC/NCEP/NWS/NOAA, College Park, MD 20740  
Email: Zhan.Zhang@noaa.gov

## 1. Introduction

The Hurricane Weather and Research Forecasting (HWRF) is one of the operational hurricane modeling systems at NCEP. It has undergone yearly upgrades and consistent improvements since its operational implementation in 2007. The HWRF-based Ensemble Prediction System (HWRF-EPS) has been improved along with its deterministic version and has been running in a real time parallel for storms in the North Atlantic basin since 2014, funded by Hurricane Forecast Improvement Project (HFIP). Over the past 5-year HFIP real time demonstration, HWRF-EPS has proven its value in many respects. The ensemble mean of HWRF-EPS outperforms its deterministic system in terms of both tropical cyclone track and intensity forecasts. HWRF-EPS also provides probabilistic forecasts, including Rapid Intensification (RI) forecasts, by representing model uncertainties in both model initial conditions and model physics.

## 2. HWRF-based Ensemble Prediction System

HWRF is the flagship operational numerical modeling system at NCEP/EMC and provides tropical cyclone (TC) forecasts in all oceanic basins. The system consists of multiple movable two-way interactive nested grids that follow the projected path of a storm. The model resolution is 13.5/4.5/1.5km in the horizontal and 75 levels in the vertical. HWRF is an atmosphere-ocean coupled system, to provide an accurate representation of air-sea interactions. An advanced vortex initialization scheme and NCEP GSI-based HWRF Data Assimilation System (HDAS) provide the means to represent the initial location, intensity, size and structure of the inner core of a hurricane and its large-scale environment.

The HWRF-EPS is configured the same as its deterministic version except for 1) the use of coarser horizontal 18/6/2km and vertical L61 resolutions; 2) Data Assimilation is turned off; 3) the use of the NCEP Global Ensemble Forecast System (GEFS) (0.5x0.5 degree) as the host model to provide model initial and lateral boundary conditions; 4) the initial TC position and intensity are perturbed to account for uncertainties in TCVitals; 5) the initial sea surface temperature (SST) field is perturbed based on a 5-year climatological GFS SST analysis and; 6) stochastic perturbations are introduced in the convection, PBL, and surface layer schemes to account for the uncertainties in model physics.

## 3. Results and Discussion

HWRF-EPS was run in real time during the hurricane season in 2018. Due to limited computing resources, not all cycles of all storms were simulated. In total, we had 159 verifiable cycles for six storms (Florence, Gordon, Isaac, Kirk, Leslie, and Michael) in the North Atlantic basin and 85 verifiable cycles for two storms (Hector and Lane) in the East Pacific basin. The ensemble averaged track and intensity from HWRF-EPS outperformed its deterministic version of HW00 (Fig. 1) by about 5% in track and 13% in intensity forecasts, respectively. Similar results have been shown in the past 5-years from earlier real-time HWRF-EPS experiments.

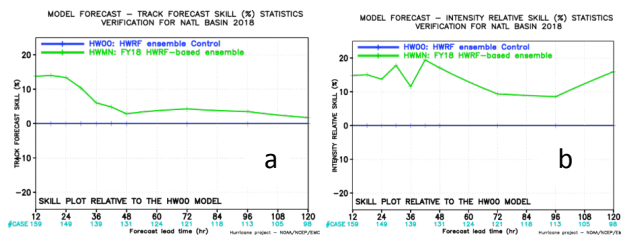


FIG. 1 Comparison of (a) track and (b) intensity forecast skill between HWRF-EPS (HWMN, green) and its deterministic version (blue).

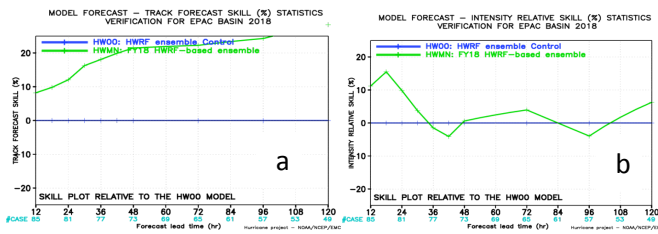


FIG. 2 As in Fig.1 except for East Pacific Basin.

For the Eastern Pacific basin, HWRf-EPS track forecasts are about 20% more skillful than its deterministic model, while having neutral impacts compared to the intensity forecasts from the deterministic version (Fig. 2). It should be noted that the sample size is too small to draw any firm conclusions.

Accurately predicting a Rapid Intensity (RI) event is one of the most difficult and challenging problems in TC intensity forecasting. Compared with the deterministic HWRf, HWRf-EPS has the advantage in forecasting RI of TCs in the form of probabilistic forecasts. Fig.3 shows an example of RI probabilistic forecasts from HWRf-EPS for Hurricane Michael. It lists all the cycles for which Hurricane Michael underwent RI compared to the RI probabilistic forecasts from the HWRf-EPS. It can be clearly seen that HWRf-EPS predicted all RI events well with high probability.

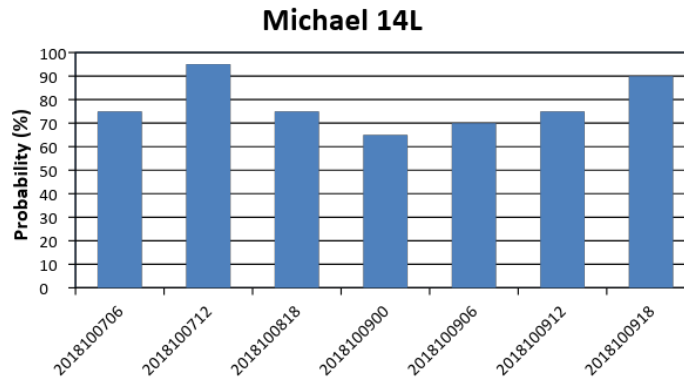


FIG. 3. Probabilistic prediction of an RI event for Hurricane Michael, 2018. The horizontal axis is the cycles where the hurricane went through RI, the vertical is the probability predicted by HWRf-EPS.

#### 4. Conclusions

HWRf-EPS has been running in real time for the last 5 years, and has demonstrated that it has always outperformed its deterministic model in terms of track and intensity forecast skill. HWRf-EPS also provides statistical information and forecast uncertainties through ensemble spread. It also demonstrated its capability to predict RI events. Further work will focus on improving the uncertainty representations in model initial conditions and model physics.

#### References:

Tallapragada V., Chanh Kieu, Y. Kwon, S., Trahan, Q. Liu, Z. Zhang, I. Kwon, 2014: Evaluation of Storm Structure from the Operational HWRf Model during 2012 Implementation. *Mon. Wea. Rev.* 142, 4308-4325.  
 Zhang Z., Vijay Tallapragada, C. Kieu, S. Trahan, and W. Wang, 2014: HWRf based Ensemble Prediction System Using Perturbations from GEFS and Stochastic Convective Trigger Function. *Tropical cyclone Research and Review*, Vol. 3, 145-161